DIRECT NUMERICAL SIMULATION OF TURBULENT CONCENTRIC ANNULAR PIPE FLOW

Seo Yoon Chung
Department of Mechanical Engineering, KAIST
373-1, Kusong-dong, Yusong-ku, Taejon, 305-701, Korea
dovecsy@kaist.ac.kr

Gwang Hoon Rhee
Department of Mechanical and Information Engineering, The University of Seoul
90, Jeonnong-dong, Dongdaemun-ku, Seoul, 130-743, Korea
ghrhee@uos.ac.kr

Hyung Jin Sung*
Department of Mechanical Engineering, KAIST
373-1, Kusong-dong, Yusong-ku, Taejon, 305-701, Korea
hjsung@kaist.ac.kr

ABSTRACT

A direct numerical simulation is performed for a turbulent concentric annular pipe flow at $Re_{D_h} = 8900$ for two radius ratios (R_1/R_2 =0.1 and 0.5). The main emphasis is placed on the transverse curvature effect on near-wall turbulent structures. Near-wall turbulent structures close to the inner and outer walls are scrutinized by computing various turbulent statistics.

INTRODUCTION

Annular pipe flow is important in engineering applications such as heat exchangers, gas-cooled nuclear reactors and drilling operations in the oil and gas industry (Nouri *et al.*, 1993). Also, annular pipe flow provides insight into the general problem of fully-developed turbulent shear flows. In the case of a concentric annular pipe flow, two boundary layers exist which have different distributions of turbulent quantities. Moreover, pipe and channel flows are the limiting cases of annular pipe flow.

A literature survey reveals that studies of turbulent concentric annular pipe flows with curvature normal to the mean flow are relatively scarce. Nouri *et al.* (1993) performed an LDV experiment in concentric and eccentric annuli for a radius ratio ($\alpha = 0.5$). Satake and Kawamura (1993) performed a large eddy simulation of concentric annular pipe flows with three radius ratios ($\alpha = 0.02, 0.04$ and 0.1). They focused on the identification of vortical structures near the inner wall. Azouz and Shirazi (1998) evaluated several turbulent models to predict the turbulent flow in concentric annuli.

The objective of the present study is to elucidate the transverse curvature effect on near-wall turbulent structure in concentric annular pipe flow. Toward this end, a direct numerical simulation is performed for a turbulent concentric annular pipe flow for two radius ratios (α =0.1 and 0.5), which exemplify the situations of strong and weak curvature effects.

NUMERICAL PROCEDURE

For an incompressible flow, the nondimensional governing equations are

$$\frac{\partial u_i}{\partial t} + \frac{\partial}{\partial x_j} u_i u_j = -\frac{\partial p}{\partial x_i} + \frac{1}{Re} \frac{\partial}{\partial x_j} \frac{\partial u_i}{\partial x_j} \quad (1)$$

$$\frac{\partial u_i}{\partial x_i} = 0 \quad (2)$$

where x_i are the cylindrical coordinates and u_i are the corresponding velocity components. All the variables are non-dimensionalized by a characteristic length (δ) and velocity scale (U_m) and Re is the Reynolds number.

*This work was supported by a grant from the National Research Laboratory of the Ministry of Science and Technology, Korea.

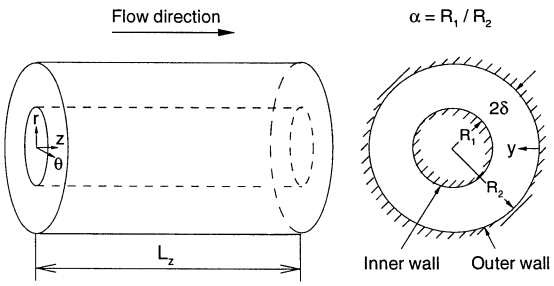

Figure 1: Schematic diagram and coordinate system.

α	0.5	0.1
Δz^+	14.30	21.07
$(R_1\Delta\theta)^+$	3.75	0.98
$(R_2\Delta\theta)^+$	7.10	7.88
Δr_i^+	0.25	0.30
Δr_o^+	0.24	0.24
Δr_{max}^+	12.96	15.27
(N_r, N_θ, N_z)	(65,128,192)	(65,256,128)

Table 1: Grid resolutions.

The governing equations (1) and (2) are integrated in time by using a fully implicit decoupling method, which has been proposed by Kim *et al.* (2000). All the terms are advanced with the Crank-Nicolson method in time and they are resolved with a second-order central difference scheme in space.

A schematic diagram and a coordinate system of the flow configuration are shown in Fig. 1. The Reynolds number based on the bulk velocity (U_m) and the hydraulic diameter (D_h) is $Re_{D_h} = 8900$. The computational length in the streamwise direction is $L_z = 18\delta$ for $\alpha = 0.5$ and $L_z = 15\delta$ for $\alpha = 0.1$, respectively. Periodic boundary conditions for velocity components are applied in the axial and circumferential directions. A no-slip boundary condition is imposed at the solid wall. As for the computational domain, a full domain is chosen for $\alpha = 0.1$. However, the computation is conducted in only one-quarter of the full cross-section for $\alpha = 0.5$. To illustrate the adequacy of the computational domains, two-point correlations of the fluctuating streamwise velocities in the streamwise (z) and azimuthal (θ) directions are investigated.

The detailed grid resolutions for two cases are listed in Table 1. The computational time step used is $0.04\delta/U_c$ and the total averaging time to obtain the statistics is $600\delta/U_c$ for both cases. Here, U_c is the laminar centerline velocity. A hyperbolic tangent distribution is used for a clustering of grid points in the wall-normal direction.

α	0.5	0.1
Re_{D_h}	8900	8900
Re_δ	3355	3487
Re_τ (Inner)	153	180
Re_τ (Outer)	144	144
C_f (Inner)	9.41×10^{-3}	1.30×10^{-2}
C_f (Outer)	8.49×10^{-3}	8.46×10^{-3}
U_c/u_τ (Inner)	22.09	19.44
U_c/u_τ (Outer)	23.26	24.10
U_m/u_τ (Inner)	14.65	12.40
U_m/u_τ (Outer)	15.43	15.38

Table 2: Mean flow parameters.

RESULTS AND DISCUSSION

To ascertain the reliability and accuracy of the present numerical simulation, the mean velocity distributions normalized by the bulk velocity are compared with the experimental data of Nouri *et al.* (1993) in Fig. 2. Agreement with the experimental data is satisfactory, although a slight deviation is observed in the center region. It is interesting to note that the integration of the measured profiles in the radial direction does not yield a value of unity while that of the numerical profiles shows 1.0. This tendency was also pointed out in the previous numerical investigation (Azouz and Shirazi, 1998). When rescaled by a process of normalization, the numerical prediction is in excellent agreement with the experimental data. Note that the positions of the maximum velocities are skewed toward the inner wall in both cases. Several mean flow parameters obtained from the present simulation are summarized in Table 2. Here, Re_δ is based on the laminar centerline velocity (U_c) and the half-width (δ) between the inner and outer wall.

Comparison is extended to the logarithmic velocity profiles in Fig. 3. In Fig. 3(a), a slight discrepancy between the profiles of the inner and outer walls appears only in the region of $y^+ > 100$. In Fig. 3(b), however, the deviations are significant and the slope of the inner profile is lower than that of the outer profile in the logarithmic region. This may be attributed to the curvature effect, which is caused by the decrease of the radius of the inner cylinder.

Root-mean-square (r.m.s.) distributions of the fluctuating velocities, normalized by the friction velocity (u_τ), are exhibited in Fig. 4. A comparison between the inner and outer walls indicates that turbulent intensities of the inner wall are smaller than those of the outer wall. This tendency is pronounced at $\alpha = 0.1$. The smaller turbulent kinetic energy in the inner wall is due to the transverse curvature effect. Since the surface area of the inner wall is smaller than that of the outer wall, the inner wall supplies relatively less turbulent kinetic

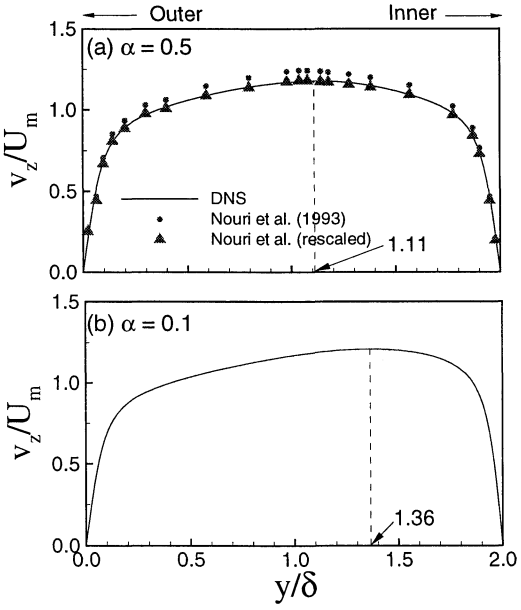

Figure 2: Mean velocity distributions.

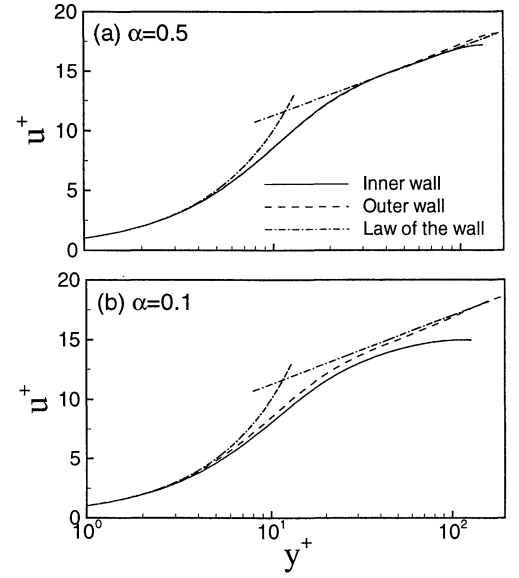

Figure 3: Mean velocity distributions for the law of the wall.

energy than the outer wall to the same volume of flow.

The Reynolds shear stress ($-\overline{v_z' v_r'}$) and total shear stress ($-\overline{v_z' v_r'} + \frac{1}{Re}\frac{dV_z}{dy}$) in the global coordinate are shown in Fig. 5(a). Here, y and v_r denote a distance from the outer wall and a velocity component normal to the outer wall, respectively. In Fig. 5(a), distributions of the Reynolds shear stress and total shear stress are asymmetric, similar to those of the mean velocities in Fig. 2. It is interesting to note that the positions of zero total shear stresses are closer to the inner walls than those of the maximum velocities (see Fig. 2). Furthermore, the distri-

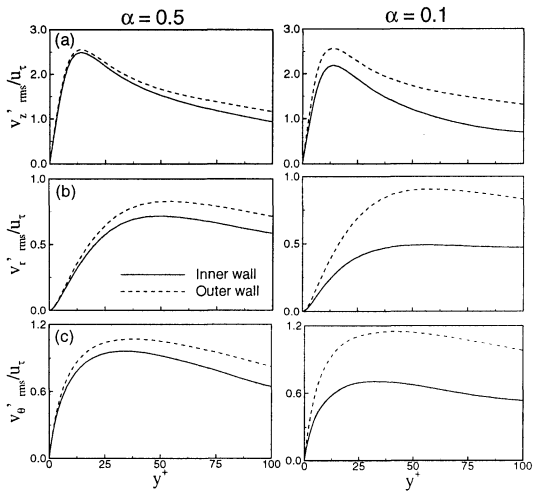

Figure 4: Root-mean-square velocity fluctuations. (a) axial velocity, (b) normal velocity and (c) azimuthal velocity.

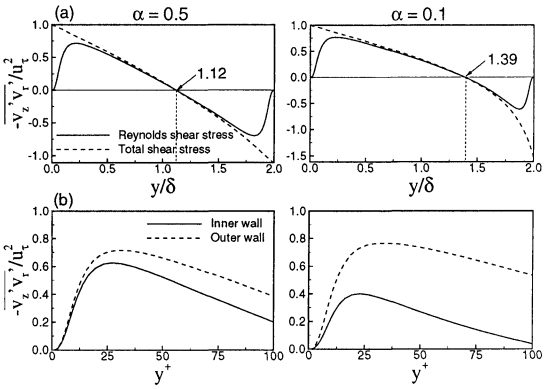

Figure 5: Distributions of Reynolds shear stress and total shear stress.

butions of the total shear stresses are slightly curvilinear due to the curvature, while these are linear in pipe and channel flows. Profiles of the Reynolds shear stress in the wall coordinate in Fig. 5(b) suggests that the Reynolds shear stress near the outer wall is larger than that near the inner wall.

The production terms in the turbulent kinetic energy budget are displayed in Fig. 6. Note that the values of the outer walls are larger than those of the inner walls for both cases. This reconfirms the results of the r.m.s. profiles of fluctuating velocities in Fig. 4.

Figure 7 shows the pressure strain terms in the budget of $\overline{u_z' u_z'}$. It is seen that the profiles of the outer wall are larger than those of the inner wall for both cases. This indicates a lower energy redistribution of the inner wall.

The skewness factors of the wall-normal velocity fluctuations are exhibited in Fig. 8. In Fig. 8(a), the skewness factor of the inner wall becomes zero at two points in contrast to that of the outer wall which has only one crossover point. These results for the inner and outer

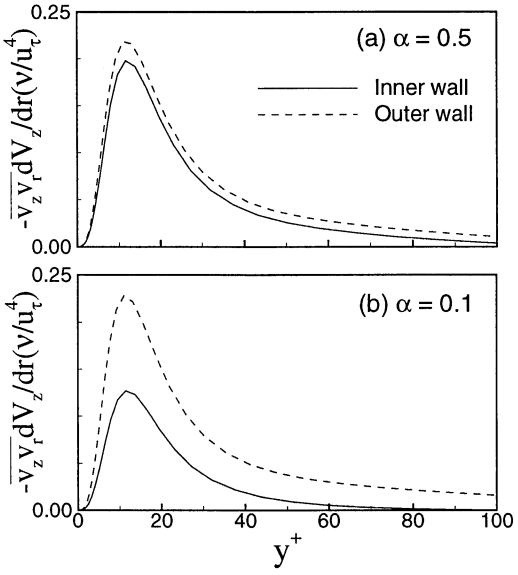

Figure 6: Production terms in the budget of the turbulent kinetic energy in wall coordinates.

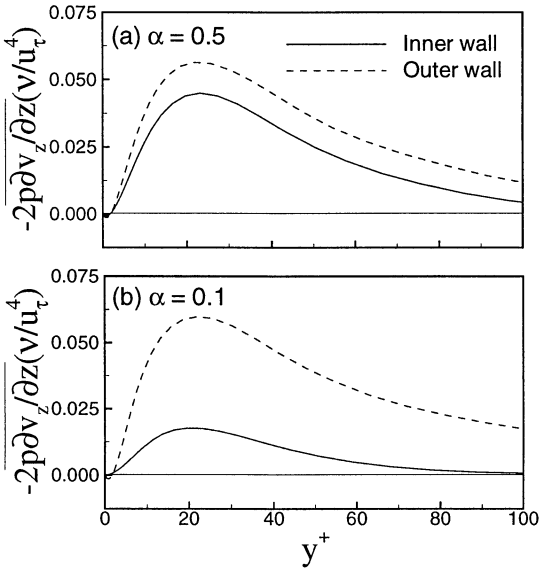

Figure 7: Pressure strain terms in the budget of $\overline{u_z' u_z'}$ in wall coordinates.

walls are consistent with the previous numerical data for channel and pipe flows corresponding to the inner and outer walls, respectively (Kim *et al.*, 1987, Eggels *et al.*, 1994). In Fig. 8(b), the profile of the skewness factor near the outer wall is similar to that in the pipe flow. Near the inner wall, however, the profile is positive throughout the layer. This tendency is discernible in the numerical simulation of turbulent boundary layer on a cylinder in an axial flow (Neves *et al.*, 1994). An examination of the results in Fig. 7 indicates that the

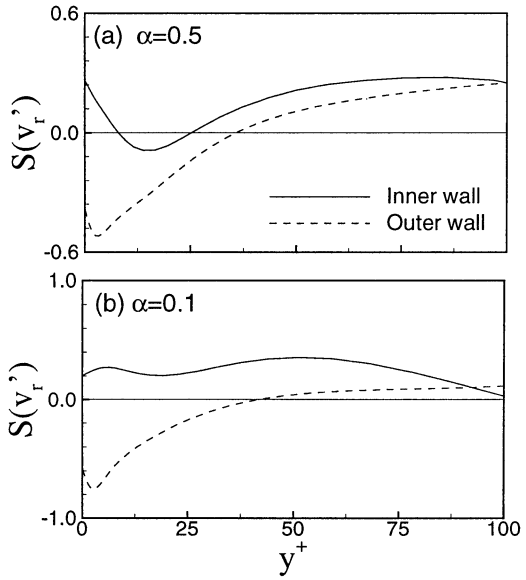

Figure 8: Skewness profiles of the wall-normal velocity fluctuations.

concentric annular pipe flow has the general characteristics of fully-developed flows such as channel and pipe flows.

To explain the altered intermittent behavior of the inner and outer walls, the flatness factors of the wall-normal velocity fluctuations are shown in Fig. 9. Near the wall ($y^+ < 20$), the values of the flatness factor near the inner and outer walls rapidly increase for both cases. This reflects the high intermittency of the wall-normal velocity fluctuations close to the wall. As reported in the numerical simulation of Xu *et al.* (1996), such high values are attributed to strong sweep events. As a result of the flatness factors of the wall-normal velocity fluctuations, the sweep events near the outer walls may be stronger than those near the inner walls.

The contribution to the Reynolds shear stress from each quadrant is shown in Fig. 10. The thin and thick lines denote the profiles of the inner wall and outer wall, respectively. The crossover points between the dominance of sweep and ejection events are located at $y^+ \approx 13$ for both cases. This is very similar to the numerical results for the channel and turbulent boundary layer on a cylinder in an axial flow (Kim *et al.*, 1987, Neves *et al.*, 1994). It is notable that sweep events near the outer walls are more predominant than those near the inner walls. On the other hand, ejections near the inner walls contribute to the Reynolds shear stress more predominantly than those near the outer walls. This can be interpreted to be the same result as that of the flatness factors

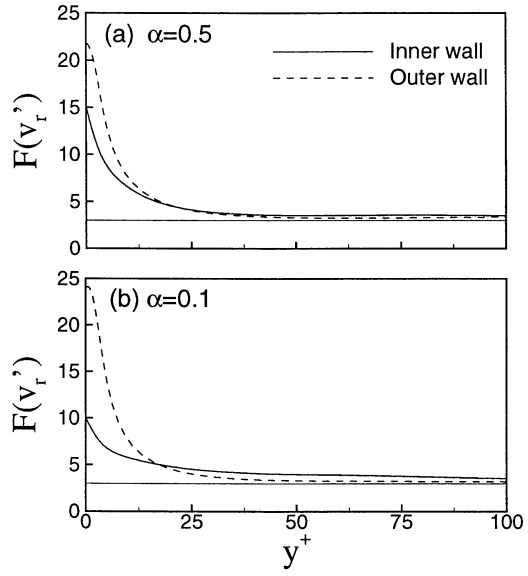

Figure 9: Flatness profiles of the wall-normal velocity fluctuations.

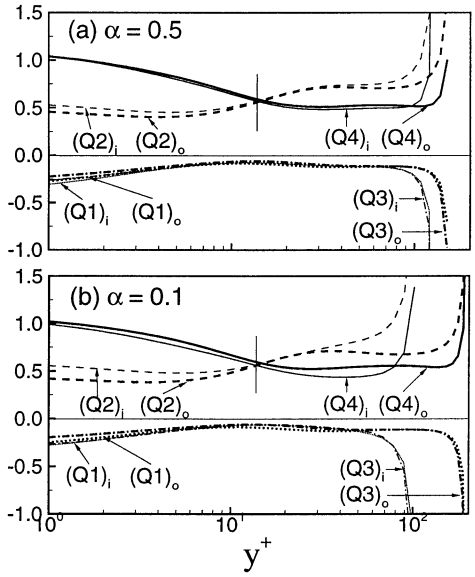

Figure 10: Reynolds shear stress for each quadrant normalized by the mean Reynolds shear stress.

of wall-normal velocity fluctuations. However, since the quadrant analysis provides not only the strength of sweep events but also the number of occurrences of sweep events, more detailed investigations are required to assess the effects of the strength of sweep events solely.

To explain the difference in the strength of sweep events between inner and outer walls more clearly, scatter plots of the instantaneous u' and v' for $\alpha = 0.1$ are illustrated in Figs. 11 and 12. Six y-locations are selected to show the altered dominance of sweep and ejection events around the crossover point, which is confirmed in Fig. 10. It should be noted that sweep events near the outer wall are much stronger than those near the inner wall. This guarantees that the strength of the sweep motions near the outer wall is higher than that near the inner wall.

To obtain a better understanding of the transverse curvature effect on the vorticity, a statistical investigation on the orientation of the vorticity field is made. Here, we follow the approach of Moin and Kim (1985). The inclination of the projection of the vorticity vector in a $r - z$ plane is given by

$$\Theta = \tan^{-1}\left(\frac{\omega_r}{\omega_z}\right). \qquad (3)$$

The probability density functions (p.d.f.s) of Θ, weighted by the magnitude of the projected vorticity vector $(\omega_r{}^2+\omega_z{}^2)/ < \omega_r{}^2+\omega_z{}^2 >$, are shown in Figs. 13 and 14. Here, $<>$ indicates the mean of the quantity inside the brackets taken on the corresponding $z - \theta$ plane. As

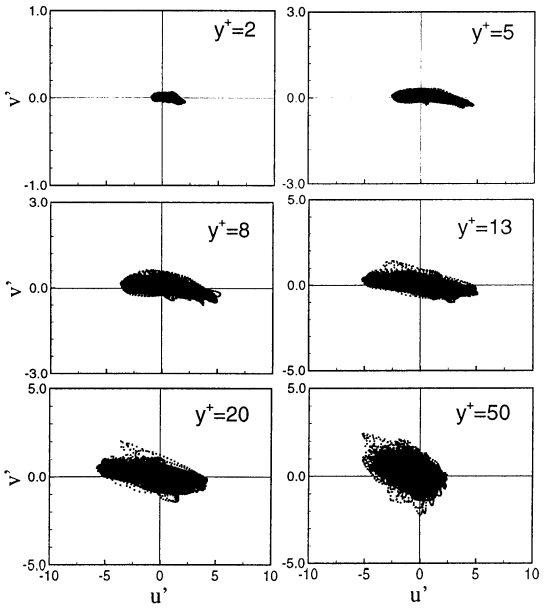

Figure 11: Instantaneous distributions of (u', v') near the inner wall for $\alpha = 0.1$.

one moves away from the wall, the peaks of the distributions are located around $\pm 90°$. This tendency persists up to $y^+ \approx 37$ in Fig. 13 and up to $y^+ \approx 10$ in Fig. 14. Farther from the wall, the peak shifts to $-135°$ and $45°$ as was observed by Moin and Kim (1985). Note that there exists a thicker layer near the outer wall, in which the vorticity has a $-135°$ and $45°$ orientation. This suggests that the vortical structures which can extract turbulent energy from the mean flow effectively are observed more frequently near the outer wall (Neves *et al.*, 1994).

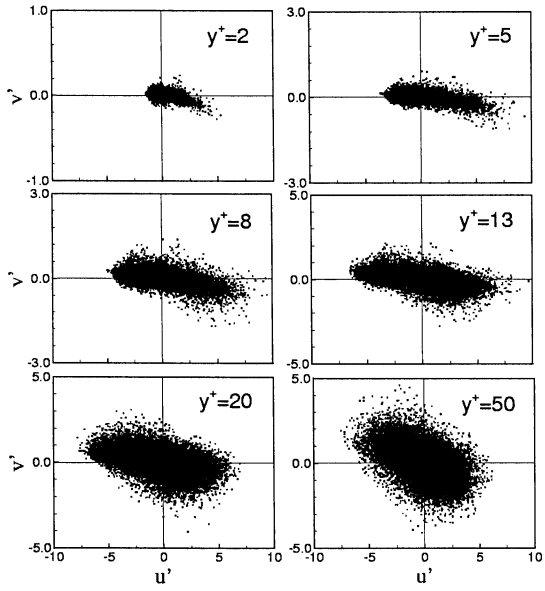

Figure 12: Instantaneous distributions of (u', v') near the outer wall for $\alpha = 0.1$.

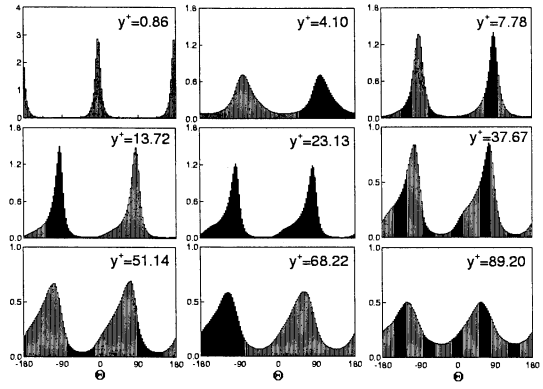

Figure 13: Weighted probability density functions of the inclination angles of the projected vorticity vectors near the inner wall for $\alpha = 0.1$.

CONCLUSION

A detailed numerical analysis has been performed to delineate the transverse curvature effects on near-wall turbulent structures in a turbulent concentric annular pipe flow. The statistical descriptions of the turbulent quantities were obtained by performing a direct numerical simulation of turbulent concentric annular pipe flow at $Re_{D_h} = 8900$ for two radius ratios ($\alpha = 0.1$ and 0.5). The present numerical results show that the turbulent structures near the outer wall are more activated than those near the inner wall.

REFERENCES

Azouz, I., and Shirazi, S. A., 1998, "Evaluation of several turbulence models for turbulent flow in concentric and eccentric annuli", *ASME J. Energ. Resour.*, Vol. 120, pp. 268-275.

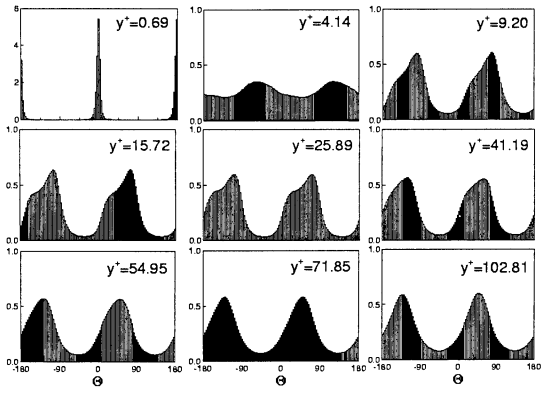

Figure 14: Weighted probability density functions of the inclination angles of the projected vorticity vectors near the outer wall for $\alpha = 0.1$.

Eggels, J. G. M., Unger, F., Weiss, M. H., Westerweel, J., Adrian, R. J., Friedrich, R., and Nieuwstadt, F. T. M., 1994, "Fully developed turbulent pipe flow: A comparison between direct numerical simulation and experiment", *J. Fluid Mech.*, Vol. 268, pp. 175-209.

Kim, J., Moin, P., and Moser, R., 1987, "Turbulence statistics in fully developed channel flow at low Reynolds number", *J. Fluid Mech.*, Vol. 177, pp. 133-166.

Kim, K., Baek, S. -J., and Sung, H. J., 2000, "An implicit velocity decoupling procedure for the incompressible Navier-Stokes equations", *Int. J. Numerical Methods in Fluids*, revised.

Moin, P., and Kim, J., 1985, "The structure of the vorticity field in turbulent channel flow. Part 1. Analysis of instantaneous fields and statistical correlations", *J. Fluid Mech.*, Vol. 155, pp. 441-464.

Neves, J. C., Moin, P., and Moser, R. D., 1994, "Effects of convex transverse curvature on wall-bounded turbulence. Part 1. The velocity and vorticity", *J. Fluid Mech.*, Vol. 272, pp. 349-381.

Nouri, J. M., Umur, H., and Whitelaw, J. H., 1993, "Flow of Newtonian and non-Newtonian fluids in concentric and eccentric annuli", *J. Fluid Mech.*, Vol. 253, pp. 617-641.

Satake, S., and Kawamura, H., 1993, "Large eddy simulation of turbulent flow in concentric annuli with a thin inner rod", *Proceedings, 9th Symposium on Turbulent Shear Flows*, Kyoto.

Xu, C., Zhang, Z., den Toonder, J. M. J., and Nieuwstadt, F. T. M., 1996, "Origin of high kurtosis levels in the viscous sublayer. Direct numerical simulation and experiment", *Phys. Fluids*, Vol. 8, pp. 1938-1944.